Reaction4Exp commented example: ^{4}He+^{208}Pb elastic and inelastic scattering

Introduction

This document describes briefly the use of the Reaction4Exp website for the case of elastic scattering. We will use as example the ^{4}He+^{208}Pb reaction. The link to the elastic scattering website is:

https://reaction4exp.us.es/elastic/index.php

1 Reminder of the optical model

In the optical model, the projectile-target interaction is described by means of an effective interaction, $U(\mathbf{R})$ (the *optical potential*). The scattering wavefunction, that describes the relative motion between the projectile and target, is a solution of a single-channel Schrodinger equation: $[H-E]\Psi(\mathbf{R})=0$ where E is the CM energy. This solution is conveniently expanded in spherical harmonics. For a *central potential* (i.e. $U=U(R)$) and *ignoring intrinsic spins*, this yields:

$$\Psi(\mathbf{K},\mathbf{R})=\frac{1}{KR}\sum_L(2L+1)i^L\chi_L(K,R)P_L(\cos\theta), \tag{1}$$

where θ is the angle between the incident momentum $\mathbf{K}$ and the final momentum $\mathbf{K'}$, which corresponds to the scattering angle in the c.m. frame.

The radial functions $\chi_L(K,R)$ are determined inserting this expansion into the Schrödinger equation, giving rise to an equation for each value of L,

$$\left[\frac{\hbar^2}{2\mu}\frac{d^2}{dR^2}-\frac{\hbar^2}{2\mu}\frac{L(L+1)}{R^2}-U(R)+E\right]\chi_L(K,R)=0, \tag{2}$$

where $U(R)$ contains both the Coulomb and nuclear potentials.

The above Schrödinger equation is solved numerically from $R=0$, starting from the value $\chi_L(K,0)=0$, and up to a maximum value (*matching radius*) $R_{\max}$. At this distance, one imposes the boundary condition:

$$\chi_L(K,R)|_{R=R_{\max}} \;=\frac{i}{2}e^{i\sigma_L}\left[H_L^{(-)}(\eta,KR_{\max})-S_LH_L^{(+)}(\eta,KR_{\max})\right] \tag{3}$$

where σ_L are the Coulomb phase-shifts and $H^{(\pm)}(\eta,KR)$ are the ingoing $(-)$ and outgoing $(+)$ Coulomb functions. From the condition (3), one determines the coefficients S_L (S-matrix elements) which, in turn, are used to compute the elastic scattering amplitude:

$$f(\theta)=f_C(\theta)+\frac{1}{2iK}\sum_L(2L+1)e^{2i\sigma_L}(S_L-1)P_L(\cos\theta) \tag{4}$$

where $f_C(\theta)$ is the scattering amplitude for pure Coulomb scattering (whose square is the Rutherford cross section).

The differential elastic cross section is evaluated according to

$$\frac{d\sigma}{d\Omega}(\theta) = |f_C(\theta) + f_N(\theta)|^2. \tag{5}$$

An important quantity is the reaction cross section, which is associated with the flux of all non-elastic channels. In terms of the S-matrix elements it is given by:

$$\sigma_{\rm reac} = \frac{\pi}{K^2}\sum_L (2L+1)(1-|S_L|^2) \tag{6}$$

where K is the cm wave number.

2 Optical model parameters

The projectile-target interaction is the sum of the Coulomb and the nuclear potentials. For the Coulomb potential, the Reaction4Exp tool uses the Coulomb interaction for a uniformly charged sphere:

$$V_c(r) = \begin{cases} \kappa \frac{Z_1 Z_2 e^2}{2R_c}\left(3 - \frac{r^2}{R_c^2}\right) & \text{if } r \le R_c \\ \kappa \frac{Z_1 Z_2 e^2}{r} & \text{if } r \ge R_c \end{cases}$$

where R_c is related to the sum of the charge radii of the colliding nuclei. Instead of using R_c directly, the Reaction4Exp website uses the so-called reduced radius, r_c, which is related to the physical radius as $R_c = r_c(A_1^{1/3} + A_2^{1/3})$, as is standard. In our working example $A_1 = 4$ and $A_2 = 208$.

For the nuclear part, we consider the following parametrization in terms of *volume* Woods-Saxon shapes, which is in fact the standard choice in the Reaction4Exp website:

$$U_{\rm nuc}(r) = -V_0 f(r, R_0, a_0) - iW_v f(r, R_i, a_i),$$

with

$$f(r, R_x, a_x) = \{1 + \exp\left[(r - R_x)/a_x\right]\}^{-1} \ .$$

We will adopt the numerical values listed in table 1. In the website, reduced radii are introduced. Then, these are converted internally to absolute (physical) radii using the projectile and target atomic numbers: $R_x = r_x(A_p^{1/3} + A_t^{1/3})$.

Figure 1 shows a screenshot of the OM parameters section in the Reaction4Exp website.

2.1 Numerical integration parameters

In addition to the optical potentials, we need to specify some additional parameters required for the numerical integration of the radial equation. Although the application sets some default values, it is convenient to check that the calculations are *converged* with respect to these parameters. In the Reaction4Exp website, we need to specify the following numerical parameters:

System	V_0 [MeV]	r_0 [fm]	a_0 [fm]	W_v [MeV]	r_i [fm]	a_i [fm]	r_c [fm]
^{4}He+^{208}Pb	96.44	1.085	0.625	32	0.958	0.42	1.2

Table 1: Woods-Saxon parameters for ^{4}He+^{208}Pb optical model. Reduced radii (r_x) are converted into absolute (physical) radii as $R_x = r_x(A_p^{1/3} + A_t^{1/3})$.

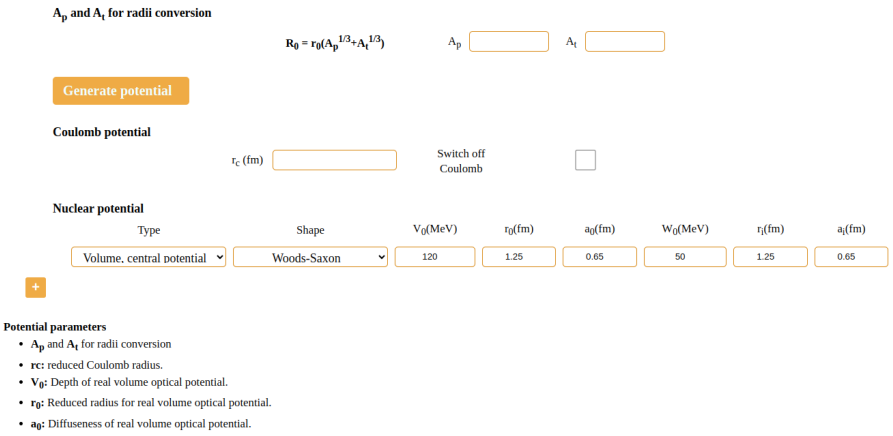

Figure 1: Optical parameters section of the Reaction4Exp website.

- **Integration step (h):** This is the radial step used for the numerical integration of the differential equation (2). It has to be chosen smaller than the diffuseness of the potentials and than the characteristic wavelength of the projectile. A simple criterion is to set $hk \leq 0.2$, where k is the wave number associated with the kinetic energy. For example, for $E_{\rm lab}$=22 MeV, $k = 2.01$ fm^{-1} and so $h \leq 0.2/2.01 = 0.1$ fm. If the integration step is too low for the considered energy, the website will show a notification. Note that too small values of h may lead to numerical instabiliites.

- **Matching radius.** This is the distance up to which the radial equations (2) are integrated. Beyond the matching radius, the code will assume that all interactions (but the monopole Coulomb one) have vanished and so the wavefunction has reached its asymptotic behaviour, given by Eq. (3). Thus, the matching radius must be chosen well outside the range of the optical potential. In our example, this potential extends up to $\approx$ 10 fm, so $R_{\rm max} \geq 20$ fm would be a "safe" choice. Note that too large values for the matching radius may lead to numerical issues.

- **Minimum and maximum total angular momentum.** The total angular momentum is the sum of the orbital angular momentum L and the spins of projectile and target: $\vec{J}_T = \vec{L} + \vec{J}_p + \vec{J}_t$. In principle, the sum in L of Eq. (4) goes from 0 to infinity. Therefore the minimum value of the angular momentum should

be set to 0 unless there is some interest in visualizing the effect of low values of L. (Even if the vector coupling $\vec{J}_p + \vec{J}_t$ is half-integer, so J_T is half-integer and its minimum value 0.5, setting the minimum value to 0 will be properly recognized by the program). In practice, convergence of the scattering observables is achieved for finite values of L since, for large values of L, $S_L \to 1$ and hence these values do not contribute to the sum (4). This occurs because, for large partial waves, the nuclear potential is negligible and the corresponding nuclear phase-shift tends to zero.

Clearly, the maximum value of L must be larger than the "grazing" angular momentum (L_g), i.e., the value of L corresponding to classical trajectories for which the nuclei start to feel the nuclear interaction. When the Coulomb force is weak, L_g can be estimated from the relation between the impact parameter and the angular momentum for a classical trajectory[1]:

$$\sqrt{L(L+1)} \approx L + \frac{1}{2} \simeq kb. \tag{7}$$

Then, L_g is estimated setting $b = R_g$, where R_g is called "grazing" or critical radius, and corresponds to the distance at which the nuclei begin to experience the nuclear interaction. The value of R_g is found to be somewhat larger than the sum of the projectile and target radii ($R_g > 1.2(A_p^{1/3} + A_t^{1/3})$ fm). A simple estimate is given by $R_g \simeq 1.45(A_p^{1/3} + A_t^{1/3})$ fm. If the deflection due to the Coulomb interaction is important, instead of Eq. (7) we may use the relation between the angular momentum and the distance of closest approach r_{min} for a classical Coulomb trajectory:

$$\sqrt{L(L+1)} \approx L + \frac{1}{2} = kr_{min}\left[1 - \frac{2\eta}{kr_{min}}\right]^{1/2} \tag{8}$$

where η is the Sommerfeld parameter. Then, we estimate L_g as the angular momentum for which $r_{min} = R_g$. Expressions (7) and (8) tell us that the number of partial waves (that is, values of L) involved in the calculation scales as the square root of the kinetic energy.

The asymptotic region will correspond to "trajectories" well beyond the grazing impact parameter so, ideally, $J_T^{\max} \sim L_{\max} \gg L_g$. This gives a hint to choose a suitable value of $J_T^{\max}$. In practice, one increases progressively $J_T^{\max}$ until convergence of the studied observable is achieved. One can also verify that the reaction cross section has dropped to 0 for $J_T^{\max}$. Note that too large values for $J_T^{\max}$ may lead to numerical problems in the calculation.

In some situations, we can estimate R_g (and hence L_g from the relations above) from the elastic angular distribution. This is the case of Fresnel and Fraunhofer scattering:

[1]This expression arises from the relation between the impact parameter and the angular momentum in a classical trajectory due to a central potential, i.e., $|\vec{L}| = m\,v\,b = p\;b$. In quantum mechanics the modulus of the angular momentum is $\sqrt{L(L+1)}\hbar$ and the linear momentum is related to the wave number by $p = \hbar k$. Then, the relation above becomes $\sqrt{L(L+1)} = kb$.

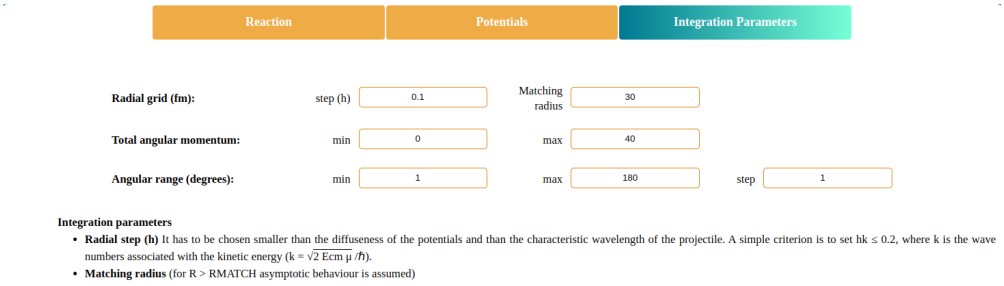

Figure 2: Numerical integration parameters section.

1. In **Fresnel** scattering, L_g is sometimes estimated as the value of L which satisfies $|S_L|$=0.5. Another common prescription is the *quarter-point* recipe. In this case, one determines a "grazing" angle, θ_g, defined as the angle for which the elastic cross section drops to 1/4 of the Rutherford cross section. From this, one estimates the grazing angular momentum as

$$L_g + 1/2 \approx \eta \cot\left(\frac{\theta_g}{2}\right) \tag{9}$$

and R_g as the distance of closest approach for that Coulomb orbit:

$$R_g = \frac{\eta}{k}\left(1 + \frac{1}{\sin(\theta_g/2)}\right) \tag{10}$$

2. In **Fraunhofer** scattering, the separation $\Delta\theta$ of successive maxima or minima gives a measure of the grazing angular momentum,

$$\Delta\theta \approx \pi/L_g, \tag{11}$$

and then R_g can be estimated from $kR_g \simeq L_g$+1/2. As in Fresnel scattering, another estimate of L_g can be obtained from the S-matrix as $|S_{L_g}|$=0.5.

Figure 2 shows a screenshoot of the R4E section for the numerical integration parameters.

3 Interpretation of the results

In Table 2 we list some kinematical parameters, namely, the wave number (k), the Sommerfeld parameter (η), and distance of closest approach in head-on Coulomb collision ($r_{\rm min}$). These quantities can be computed with the expressions,

$$k = \sqrt{\frac{2\mu E_{\rm cm}}{\hbar^2}} = \sqrt{\frac{2\mu E_{\rm lab}}{\hbar^2}\frac{A_t}{A_t + A_p}}; \qquad \eta = \frac{Z_p Z_t e^2}{\hbar v} = \frac{Z_p Z_t e^2 \mu}{\hbar^2 k}; \qquad r_{\rm min} = \kappa\frac{Z_1 Z_2 e^2}{E_{\rm cm}}$$

where $\kappa = 1/(4\pi\epsilon_0)$. Note that this expression is more easily evaluated in a system of units with $\kappa = 1$.

$E_{\rm lab}$ (MeV)	$E_{\rm cm}$ (MeV)	k (fm^{-1})	η	$r_{\rm min}$ (fm)
5	4.91	0.960	23.1	48.1
10	9.81	1.36	16.3	24.1
22	21.6	2.01	11.0	10.9
27	26.5	2.23	9.94	8.9
60	58.9	3.32	6.67	4.0

Table 2: Useful kinematical parameters for the ^{4}He+^{208}Pb reaction at several incident energies. The parameters k, η and $r_{\rm min}$ correspond, respectively, to the wave number, the Sommerfeld parameter, and the distance of closest approach for a head-on collision.

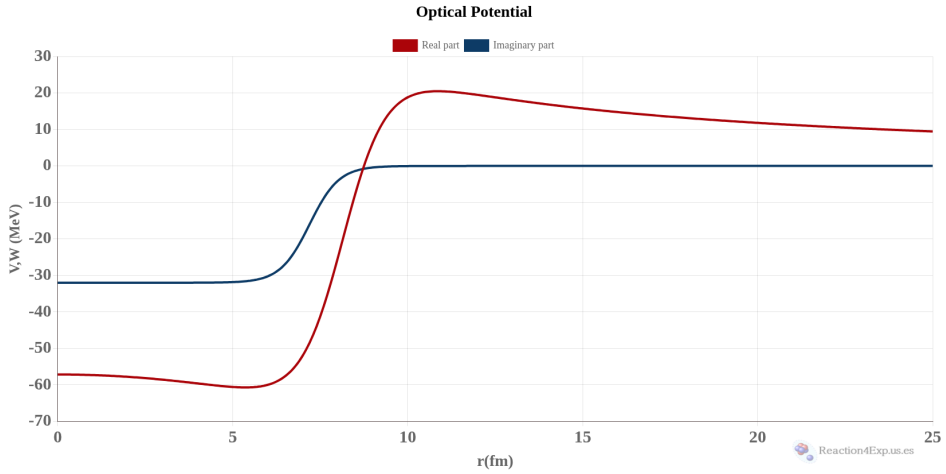

Figure 3: Real and imaginary parts of the optical potential, as displayed by the Reaction4Exp website.

3.1 Coulomb barrier

The nominal height of the Coulomb barrier can be estimated from the maximum of the real (Coulomb plus nuclear) potential. According to Fig. 3 we see that this is around 22 MeV. This is consistent with the simple estimate:

$$V_b \approx \frac{Z_1 Z_2 e^2}{R_b}; \qquad R_b \approx 1.44(A_1^{1/3} + A_2^{1/3}) \text{ fm}$$

which, in this case, gives $V_b \approx 21.8$ MeV and $R_b = 10.8$ fm.

3.2 Differential cross sections

The elastic differential cross section is shown in Fig. 4 for several incident energies: 10, 22, 27 and 60 MeV, plotted relative to the Rutherford cross section. We can see that:

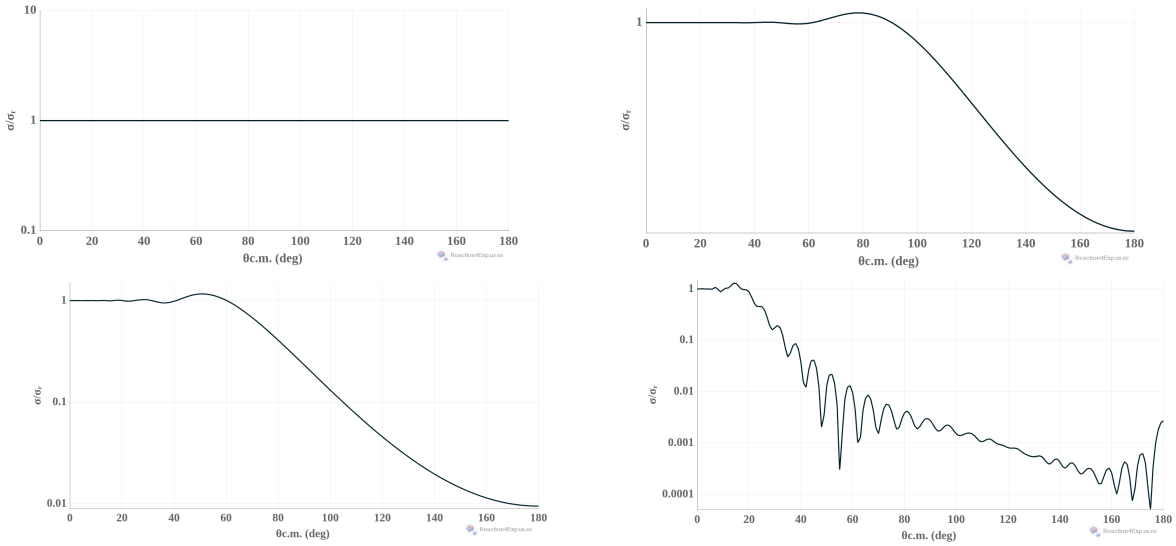

Figure 4: Elastic differential cross sections relative to Rutherford cross section at $E_{\rm lab}$=10, 22, 27 and 60 MeV (from left to right and top to bottom).

- At E=10 MeV, the ratio is almost 1, that is, we are in a situation of **pure Coulomb scattering** and is well described by the Rutherford formula. At this energy, the projectile does not *feel* the nuclear interaction. This is consistent with large value of $r_{\rm min}$ listed in Table 2.
- At E=22 MeV, the distribution departs from the Rutherford formula, as a consequence of the nuclear interaction. Beyond a certain angle ($\theta_{\rm c.m.} \approx 60^\circ$), the cross section drops quickly. This is typical of the "shadow" region observed in diffraction that occurs in Fresnel scattering.
- At E=27 MeV, the elastic angular distribution displays a typical **Fresnel** diffraction pattern. We recall that a prerequisite for the observation of this pattern is that $L_g \gg 1$ and $\eta \gg 1$. According to Table 2, at this energy $\eta = 8.9$, so the latter condition is fulfilled. The grazing angular momentum can be estimated from the condition $|S_L| = 0.5$ which occurs for $L \simeq 10$.
- At E=60 MeV, the angular distribution displays a more oscillatory structure, thus departing from the Fresnel pattern and approaching to what we have called **Fraunhofer** scattering.

3.3 S-matrix elements

Reaction4Exp provides also the nuclear S-matrix[2], which is related to the coefficient of the outgoing waves for a given partial wave L [see Eq. (3)]. This is usually expressed as

$$S_L = e^{2i\delta_L},$$

[2]More precisely, the Coulomb modified nuclear S-matrix

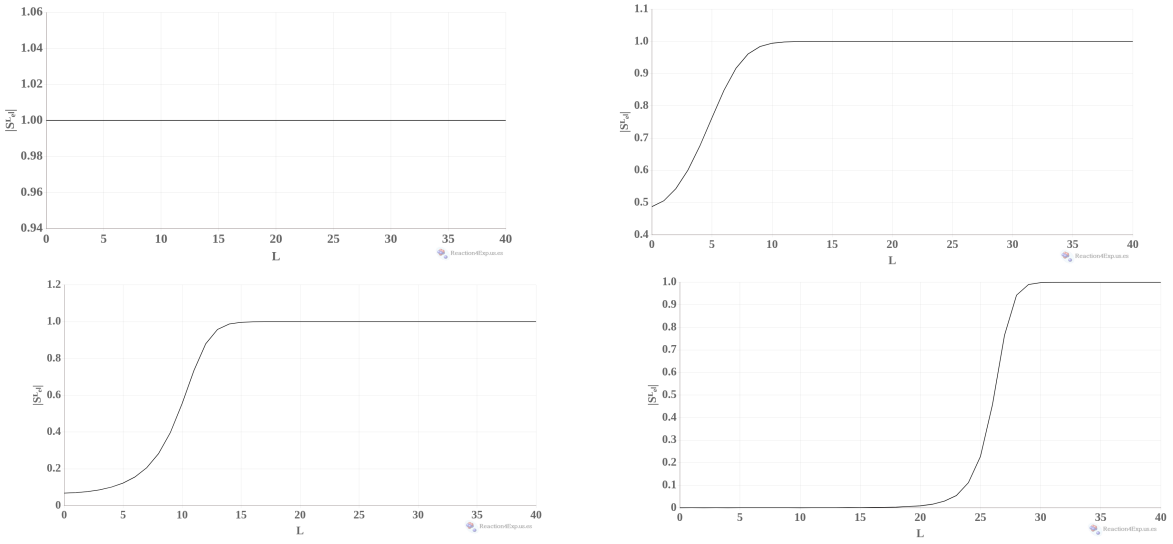

Figure 5: Modulus of the elastic S-matrix as a function of the total angular momentum J_T for energies $E_{\rm lab}$=10, 22, 27 and 60 MeV (from left to right and top to bottom).

where δ_L are the *phase shifts* of the Lth partial wave. Let us recall some properties of the S-matrix and their associated phase shifts:

- In absence of nuclear potentials $\delta_L = 0$ and $S_L = 1\ \forall L$
- If there are only real potentials, $|S_L| = 1\ \forall L$.
- When an imaginary potential is present, $|S_L| < 1$ for small L but, for large L, $|S_L| \to 1$.

The fact that $|S_L| < 1$ for small values of L reflects the loss of flux caused by the imaginary potential. Classically, it can be understood through the relation (7) and (8). Small impact parameters correspond to closer trajectories, and hence to a higher sensitivity to the short-range potentials.

The Reaction4Exp website provides the modulus of the S-matrix. As an example, we plot in Fig. 5, the modulus of the S-matrix at four different energies: 10, 22, 27 and 60 MeV. We see that:

- At $E = 10$ MeV, the modulus is almost 1 for all partial waves. This is telling us that there is no effect from the nuclear potential.
- At E=22, 27 and 60 MeV, there is a range of values of L for which $|S_L| < 1$. Moreover, this absorptive effect becomes more important for increasing incident energy.
- The range of values of L for which $|S_L| < 1$ increases for increasing energy. This can be understood as the increase of the grazing angular momentum with increasing incident energy, according to Eq. (7).

Reaction4Exp also provides the Argand plot and the phaseshifts as a function of J, but they will not be discussed at this point.

3.4 Near-side and far-side decomposition of the elastic cross section

In addition to the elastic cross section the Reaction4Exp website provides also the *nearside* and *farside* components. In Fig. 6 this decomposition is shown for the 3 energies considered above. We can see that:

- At 10 and 27 MeV, the cross section is almost entirely due to the nearside trajectories.
- At E=60 MeV, there are smooth regions dominated by either the *nearside* or the *farside* components. However, around $\theta_{\rm cm} \approx 60^\circ$ and $\theta_{\rm cm} \approx 170^\circ$ both components have similar magnitude, and their interference produces the observed oscillations in the elastic scattering.

4 Inelastic scattering: ^{4}He+^{208}Pb $\rightarrow$ ^{4}He+^{208}Pb(3^-) at 23.5 MeV

This document describes briefly the use of the Reaction4Exp website for the case of inelastic scattering. We will use as example the ^{4}He+^{208}Pb $\rightarrow$ ^{4}He+^{208}Pb(3^-) reaction at 23.5 MeV. This physics case is taken from the reference of Lilley *et al*, Nuclear Physics A342, p. 165 (1980), Ref. I hereafter.

The link to the inelastic scattering website is:
`https://reaction4exp.us.es/cc_fresco/fresco_cc.php`

5 Brief reminder of the DWBA approximation

To describe an inelastic process of the form $a + A \rightarrow a + A^*$ (target excitation) within the DWBA approximation the projectile–target interaction is conveniently written as:

$$V(\mathbf{R}, \xi) = V_0(R) + \Delta V(\mathbf{R}, \xi), \tag{12}$$

where $V_0(R)$ contains in general nuclear and Coulomb parts, and describes the relative motion of the projectile and target, and $\Delta(\mathbf{R}, \xi)$ is the part of the projectile–target interaction which is responsible for the inelastic process. It depends on the internal coordinates of the nucleus being excited ($\{\xi\}$) as well as on the projectile–target relative coordinate ($\mathbf{R}$).

We consider that the target nucleus is initially in its ground state, described by some wavefunction $\phi_i(\xi)$, and is excited to some state $\phi_f(\xi)$. Within the DWBA approximation, the scattering amplitude for this process is given by:

$$\boxed{f_{fi}(\theta) = -\frac{\mu}{2\pi\hbar^2} \int d\mathbf{R}\ \chi_f^{(-)*}(\mathbf{K}_f, \mathbf{R}) \Delta V_{if}(\mathbf{R}) \chi_i^{(+)}(\mathbf{K}_i, \mathbf{R}),} \tag{13}$$

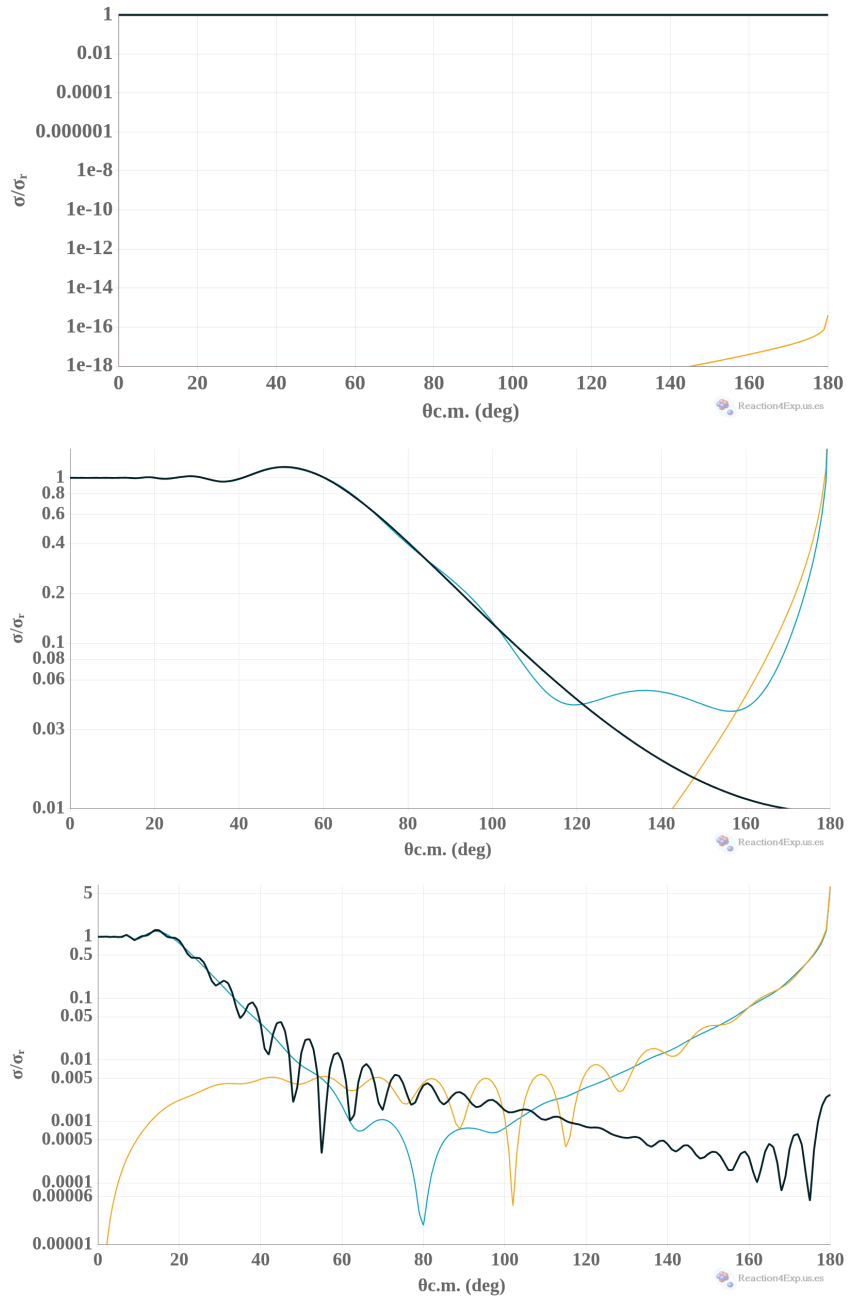

Figure 6: Far-side (orange) /near-side (blue) decomposition of the elastic cross cross section ^{4}He+^{208}Pb at $E_{\rm lab}$=10, 27 and 60 MeV (top to bottom).

where θ is the scattering angle (in c.m. frame) and $\Delta V_{if}(\mathbf{R})$ is the *transition potential*

$$\boxed{\Delta V_{if}(\mathbf{R}) = \int d\xi \phi_f^*(\xi) \Delta V(\xi, \mathbf{R}) \phi_i(\xi).} \tag{14}$$

In Eq. (13), $\chi_i^{(+)}(\mathbf{K}_i, \mathbf{R})$ is the distorted-wave describing the projectile-target relative motion in the incident channel. This distorted-wave is the solution of the Schrödinger equation with the average potential $V_0(R)$:

$$\left[-\frac{\hbar^2}{2\mu_{aA}} \nabla^2_{\mathbf{R}} + V_0(R) - E_i \right] \chi_i^{(+)}(\mathbf{K}_i, \mathbf{R}) = 0 \tag{15}$$

where E_i is the c.m. kinetic energy in the entrance channel. Typically, the nuclear part of the optical potential $V_0(R)$ is parametrized in terms of some convenient form (e.g. Woods-Saxon shape) and the parameters adjusted to reproduce the elastic angular distribution. Analogously, $\chi_f^{(-)}(\mathbf{K}_i, \mathbf{R})$ is the corresponding distorted wave for the final channel. In practice, we use the same potential as for the incident channel.

6 Radial formfactors in the collective model

In many practical situations, such as in the collective models considered here, it is possible to write:

$$\Delta V(\mathbf{R}, \xi) = \sum_{\lambda > 0} \mathcal{F}_\lambda(R) \sum_\mu \mathcal{T}_{\lambda,\mu}(\xi) Y_{\lambda\mu}(\hat{R}) \tag{16}$$

The transition potential is given by:

$$\Delta V_{if}(\mathbf{R}) \equiv \langle I_f M_f | \Delta V(\mathbf{R}, \xi) | I_i M_i \rangle = \sum_{\lambda > 0} \mathcal{F}_\lambda(R) \langle I_f M_f | \mathcal{T}_{\lambda\mu}(\xi) | I_i M_i \rangle Y_{\lambda\mu}(\hat{R}) \tag{17}$$

where the *formfactor* $\mathcal{F}_\lambda(R)$ contains the radial dependence and $\mathcal{T}_{\lambda\mu}$ is a given multipole operator depending on the structure model. Using the Wigner-Eckart theorem:

$$\langle I_f M_f | \mathcal{T}_{\lambda\mu}(\xi) | I_i M_i \rangle = (2I_f + 1)^{-1/2} \langle I_f M_f | I_i M_i \lambda\mu \rangle \langle I_f \| \mathcal{T}_\lambda(\xi) \| I_i \rangle_{\mathrm{BM}} \tag{18}$$

where $\langle I_f \| \mathcal{T}_\lambda(\xi) \| I_i \rangle$ are the so-called reduced matrix elements.

We consider two important cases:

6.1 Coulomb excitations

The coupling potentials are given by:

$$\Delta V_{if}(\mathbf{R}) \equiv \langle f; I_f M_f | \Delta V | i; I_i M_i \rangle = \sum_{\lambda > 0, \mu} \frac{4\pi\kappa}{2\lambda + 1} \frac{Z_t e}{R^{\lambda+1}} \langle f; I_f M_f | \mathcal{M}(E\lambda, \mu) | i; I_i M_i \rangle Y_{\lambda\mu}(\hat{R}) \tag{19}$$

where we see that $\mathcal{T}_{\lambda,\mu} \rightarrow \mathcal{M}(E\lambda,\mu)$ is the electric multipole operator. Its reduced matrix elements are related to the electric transition probability

$$B(E\lambda; i \rightarrow f) = \frac{1}{2I_i+1}|\langle f; I_f||\mathcal{M}(E\lambda)||i; I_i\rangle|^2. \tag{20}$$

In the collective rotor model, the $B(E\lambda)$ value can be related to the so-called **intrinsic reduced matrix element** ($Mn(E\lambda)$):

$$\sqrt{B(E\lambda; I_i \rightarrow I_f)} = i^{I_i-I_f+|I_i-I_f|}\langle I_i K\lambda 0|I_f K\rangle Mn(E\lambda) \tag{21}$$

where K is the bandhead for the rotational band (for low-lying states of even-even nuclei K is usually 0). If the initial state has spin $I_i = 0$, then $Mn(E\lambda) = \pm\sqrt{B(E\lambda; 0 \rightarrow I_f)}$.

6.2 Nuclear excitations

For small nuclear deformations the projectile-target nuclear interaction can be expanded as:

$$V(\mathbf{R},\xi) \simeq V(R-R_0) - \sum_{\lambda,\mu}\hat{\delta}_{\lambda\mu}\frac{dV(R-R_0)}{dR}Y_{\lambda\mu}(\theta,\phi) + \ldots \tag{22}$$

where $\hat{\delta}_\lambda$ are deformation length operators. Hence, the transition potentials for nuclear excitations (with $\lambda > 0$) are

$$V_{if}(\mathbf{R}) = -\frac{dV(R-R_0)}{dR}\langle f; I_f M_f|\hat{\delta}_{\lambda\mu}|i; I_i M_i\rangle Y_{\lambda\mu}(\hat{R}) \tag{23}$$

The required structure input are the reduced matrix elements of the deformation operator which, in Reaction4Exp is given as a signed real number, the deformation length:

$$\langle f; KI_f\|\hat{\delta}_\lambda\|i; KI_i\rangle = \delta_\lambda\langle I_i K\lambda 0|I_f K\rangle \tag{24}$$

Note that, in the rotor model, the sign of δ_λ and $Mn(E\lambda)$ is the same. The Reaction4Exp calculations require the $Mn(E\lambda)$ and δ_λ parameters.

In general, both the Coulomb and nuclear interactions will contribute to the excitation and so the transition potential will be the sum of the nuclear and Coulomb transition potentials and, consequently, the corresponding scattering amplitude will be given by the coherent sum of the individual nuclear and Coulomb amplitudes, i.e.,

$$f_{if}(\theta) = f_{if}^{N}(\theta) + f_{if}^{\mathrm{C}}(\theta). \tag{25}$$

Since the corresponding inelastic cross section is proportional to the square of $f_{if}(\theta)$, interference effects will occur between the nuclear and Coulomb parts.

It is common to use a dimensionless parameter, the deformation parameter β, to describe the deformation, which can be related to the inputs for the Reaction4Exp calculations through:

23.5 MeV Woods-Saxon optical potentials

Set	a_R	R_R	V_R	a_I	R_I	W_V	W_S	$V(11)$	$W(11)$	χ^2/pt
A	0.50	1.464	110.9	0.203	0.784		157.7	1.05	0.047	0.74
B	0.55	1.449	86.89	0.653	1.251	11.325		1.06	0.047	0.88
C	0.625	1.384	92.5	0.592	1.265		22.24	1.04	0.24	0.79
D	0.70	1.298	117.5	0.601	1.308		17.98	1.03	0.32	0.77

Figure 7: Optical model parameters from Lilley et al, NPA 342, 165 (1980).

$$\beta_C = \frac{4\pi\langle I_i K\lambda 0|I_f K\rangle Mn(E\lambda)}{3ZeR_c^\lambda} \tag{26}$$

$$\beta_N = \frac{\delta_\lambda}{R_n}, \tag{27}$$

where Z is the charge of the deformed nucleus, R_c its average charge radius and R_n its average mass radius.

7 Reaction4Exp calculations

For the Reaction4Exp calculations, we will use the optical model potential C of Table 1 of Lilley *et al* (see Fig. 7). The considered excitation, $0^+ \to 3^-$ has necessarily $\lambda = 3$ so we will need the corresponding intrinsic reduced Coulomb matrix element and nuclear deformation length. Note that the reduced radius is defined as $R = R_{R(I)}A_T^{1/3}$ so in React4Exp $A_p = 0$ and $A_t = 208$

For the Coulomb part, we will consider a reduced Coulomb radius $r_C = 1.2$ fm and a value for $\beta_C = 0.113$, taken from Table 2 in Ref 1 for potential set C. The deformation can be extracted from this table as well $\delta_N = \beta_N R_N = 0.85$ fm.

Some important issues to take into account for a correct implementation of these calculations:

- The energy of the first 3^- state of ^{208}Pb can be consulted in *https://www.nndc.bnl.gov/nudat3/*
- In this case the target is the one excited. As such the parameters for the deformation must be given for the target. As well, only the deformation for $\lambda = 3$ is relevant in this calculation.
- A large value for the maximum total angular momentum $J_T > 100$ is required for convergence. Make sure to set *absend* to -1 to avoid an early cutoff.

The results obtained for the elastic and inelastic cross sections are displayed in Fig. 8.

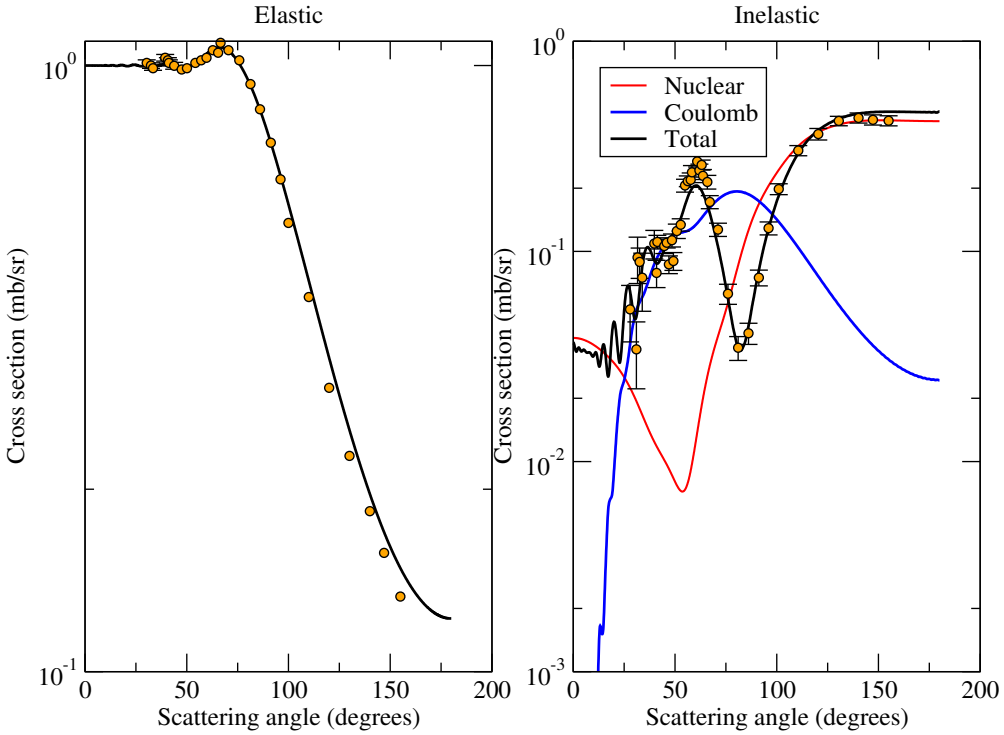

Figure 8: Left: Elastic differential cross section (relative to Rutherford cross section). Right: inelastic differential cross section.

It is illustrative to study the separate effect of the Coulomb and nuclear couplings in the inelastic cross sections. For this purpose, we can set to zero the corresponding input in the calculation. The results are also included in Fig. 8. From these curves, several conclusions can be drawn:

- The Coulomb excitation mechanism is dominant at intermediate angles, whereas the nuclear excitation dominates the larger and smaller scattering angles. This is a direct consequence of the "long-range" versus "short-range" nature of these interactions and to the sharp decrease of Coulomb excitation at small angles.
- Around $\theta_{\text{c.m.}} \approx 25^\circ$ and 75° the Coulomb and nuclear cross sections are of similar magnitude, and hence the interference effect between both contributions is apparent at these angles. Moreover, we see that this interference presents both constructive and destructive effects.